Available online at www.sciencedirect.com
SCIENCE DIRECT®
International Journal of Thermal Sciences 44 (2005) 709–719
International Journal of Thermal Sciences
www.elsevier.com/locate/ijts

A quantitative IR thermographic method to study the laminar separation bubble phenomenon

R. Ricci [a], S. Montelpare [b,*]

[a] *University of Chieti, PRICOS, Viale Pindaro 42, Pescara, Italy*
[b] *Università Politecnica delle Marche, Department of Energetics, Via Brecce Bianche, 60100 Ancona, Italy*

Received 4 November 2004; received in revised form 1 February 2005; accepted 15 February 2005

Available online 14 April 2005

Abstract

The boundary layer separation phenomena are present in many application fields: for example the sailplanes, the micro-vehicles, the small wind turbines, the airplanes and the cars. On aerodynamic bodies operating at low Reynolds numbers, lesser than one million, it may happen a boundary layer local separation defined as: laminar separation bubble. This phenomenon induces a body drag increase and an eventual lift decrease; in some situations the cyclical bubble formation and detachment may induce pressure pulses and consequent vibration phenomena. In a previous research work [Internat. J. Thermal Sci. 43 (2004) 315] was verified the possibility to show qualitatively the presence of a laminar bubble by means of a thermographic observation of the body surface. In this work is verified the possibility to carry out a quantitative study of the laminar bubble phenomenon by using the same IR technique. Three characteristic points of the bubble are particularly studied: the laminar separation point, the transition point and the turbulent reattachment point. The laminar bubble behaviour is analysed on a RR3823HL airfoil by varying the angle of attack and the Reynolds number; the adimensional Stanton number, based on the airfoil chord, is obtained in order to individuate the requested points in a more simple and objective way. This adimensional number is carried out by means of a finite numerical difference approach that makes a balance among the heat fluxes on the airfoil surface.

Keywords: Laminar separation bubble; Infrared thermography; Stanton number; Low Reynolds number; Wind turbine; Sailplane; Micro-vehicles

1. Introduction

The laminar bubble phenomenon studied in this research is present in many application fields like the sailplanes, the microvehicles, the cars and the small wind turbines; the presence of a local boundary layer separation induces an airfoil aerodynamics drag increase and eventually a lift decrease. In some situations the laminar bubble may cyclically detach from the wing surface inducing a pressure pulse; this may cause a mechanical vibration. It is so necessary to destroy or reduce this phenomenon by means of dedicated systems: turbulators, acoustic excitation, vibrational excitation. In this order, it is useful to know and foresee the laminar bubble behaviour, by varying the angle of attack and the Reynolds number; so the bubble position and dimension should be known as functions of alfa and *Re*.

The Laminar bubble (Fig. 1) is a local boundary layer separation phenomenon that is mainly present at low Reynolds number. The bubble forms under three subsequent conditions:

- formerly there is a laminar boundary layer separation in presence of an adverse pressure gradient;
- subsequently there is a free shear layer transition;
- finally there is a turbulent reattachment downstream the laminar separation point.

Under these conditions it forms on the body surface a three-dimensional zone having a pressure about uniform due to the recirculating flow inside the bubble. The laminar separation bubble (LSB) phenomenon was investigated by

* Corresponding author.
E-mail address: s.montelpare@ing.univpm.it (S. Montelpare).

1290-0729/$ – see front matter
doi:10.1016/j.ijthermalsci.2005.02.013

Nomenclature

A	wavelength amplitude	m
B_S	laminar separation point	
B_T	transition point	
B_R	turbulent reattachment point	
c	airfoil chord length	m
C_L	wing lift coefficient	
C_D	wing drag coefficient	
$C_{M,c/4}$	wing pitching moment coefficient	
c_p	airfoil pressure coefficient	
D	drag	N
h	convective heat transfer coefficient	$W{\cdot}m^{-2}{\cdot}K^{-1}$
H	shape factor	
L	lift	N
L_E	separation point distance from the leading edge	m
L_T	bubble transition length	m
M	moment	$N{\cdot}m$
Nu	Nusselt number	
q_∞	free stream dynamic pressure	$N{\cdot}m^{-2}$
Re	Reynolds number	
S	wing section planform area	m^2
Pr	Prandtl number	
St	Stanton number	
St_{U_e}	Stanton number based on the U_e velocity	
U_e	inviscid velocity outside the boundary layer	$m{\cdot}s^{-1}$
U_∞	free stream velocity	$m{\cdot}s^{-1}$

Greek symbols

α	angle of attack	°degrees
δ_{kin}	kinetic boundary layer thickness	m
δ^*	thickness displacement	m
λ	thermal conductivity	$W{\cdot}m^{-1}{\cdot}K^{-1}$
Λ	Polhausen parameter	
μ	dynamic viscosity	$kg{\cdot}s^{-1}{\cdot}m^{-1}$
ν	kinematic viscosity	$m^2{\cdot}s^{-1}$
ρ	density	$kg{\cdot}m^{-3}$
θ	momentum thickness displacement	m

Subscripts

∞	conditions of the free stream
m	mean value
w	conditions on the wall

Superscript

$'$	value referred to the airfoil section

several authors [1–3,9–12] and it was widely analysed. Some of the measurement techniques normally used to evaluate the bubble presence are the load balance, the c_p distribution analysis and the flow visualizations [1–12]. The load balance method reveals the bubble presence as a drag increase and sometime as a $C_L - \alpha$ curve slope variation [13]; by using this technique it is possible to evaluate the alfa (α) range corresponding to a LSB presence but there is no possibility to carry out information about the bubble length and position. The c_p distribution analysis allows to individuate the bubble presence from the pressure plateau inside the pressure recovery zones; this method permits an evaluation of the bubble length and position, but do not give information about the transversal bubble dimension and it is not accurate to estimate the laminar separation, the transition and the turbulent reattachment points. Finally the flow visualizations are good for qualitative investigations but do not offer quantitative data. This paper meant to present a different measure technique to qualitatively evaluate the bubble presence [14] and to obtain quantitative information about its characteristic points: i.e. the laminar separation, the transition and the turbulent reattachment points. A previous work [14] verified the possibility to use a thermographic method to localize the bubble presence; this was carried out also by comparing the thermographic images with the c_p distribution analysis. In the present work is carried out a quantitative analysis of the bubble behaviour; the thermographic data are so implemented in a finite difference model and subsequently processed in order to obtain the Stanton number behaviour along the airfoil chord. The individuation of singular points in the

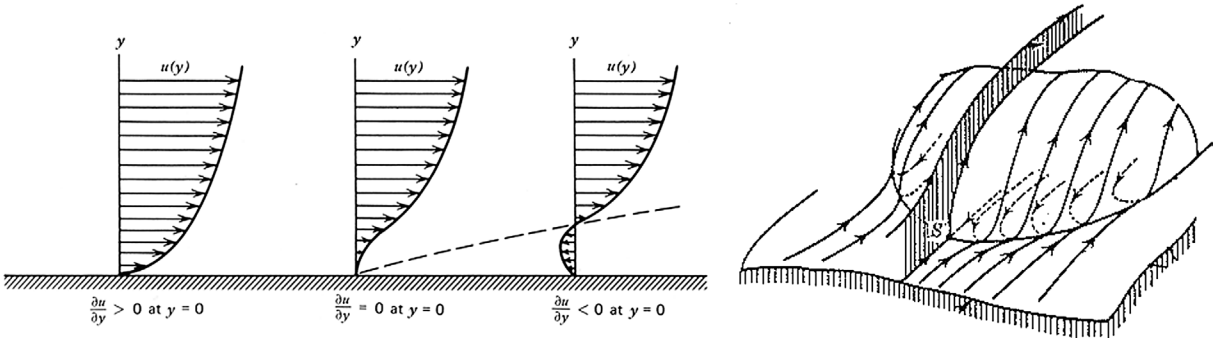

Fig. 1. The laminar separation bubble.

Stanton distribution allows a determination, more objective as possible, of the three quantities characterizing the bubble: the laminar separation point B_S, the transition point B_T and the turbulent reattach B_R. The study of these three quantities by varying the angles of attack and the Reynolds number allows a greater understand of the laminar bubble phenomenon in order to avoid its presence or to reduce its effects. The thermographic analyses are supported by the computational software XFOIL and by theoretical approaches.

2. The experimental setup

The experimental apparatus used in this research is composed by different facilities: a subsonic wind tunnel, an infrared camera, a wing section cutting machine, a load balance and a simultaneous multipressure scanning system.

The wind tunnel (Fig. 2) available by the "Dipartimento di Energetica dell'Università Politecnica della Marche" is an open circuit subsonic gallery having the subsequent main characteristics:

- the test section dimensions are: 620 (W) × 380 (H) × 1500 (L) mm;
- the inlet test section area contraction ratio is 4.65;
- the inlet maximum velocity is 38 $m \cdot s^{-1}$;
- the mean turbulence in the inlet section is 0.3%;
- the fan power has a power of 5.5 kW and the revolutions number are controlled by an inverter.

The IR camera is a FLIR SC3000 focal plane array (Fig. 3(a)) having a thermal resolution of 30 [mK] and a sensor array of 320 × 240 pixel; the thermographic images are acquired by means of a PCMCIA card that allows to obtain a maximum scan rate of 50 Hz. In this work the thermograms are captured at a frequency of 8 Hz and in number of 50 frames; this allows a post processing of image by means of a program developed under Matlab (Fig. 4). This cleans the thermographic image from noises due to:

the low temperature difference between the wing section surface and the background;
the periodic automatic shutting performed by the IR camera to erase the internal offset among the sensor array.

The thermal noise is reduced by first averaging the 50 acquired thermal images; successively a further image manipulation is carried out by means of a specific filter that removes the temperature spikes lesser than 30 mK between two contiguous pixel (i.e. lesser than the IR camera minimal thermal resolution). This Matlab procedure introduces an error related to the chord length and so to the positions of the points of interest; this is due to the uncertainty in the determination of the first pixel, corresponding to the airfoil leading edge, and of the last pixel, corresponding to the trailing edge, from the thermographic image. This error was evaluated as the 1% of the chord and so the B_S, B_T, B_R points are to be considered with an error of $\pm 1\%$ of the chord.

The IR camera is placed over the wind tunnel test section in order to observe the wing section extrados trough an infrared window (Fig. 3(b)); this is realized with a polyethylene foil having a thickness of some ten micron and a transmission coefficient, in the thermal camera wavelength (8–9 micron), of 0.96.

The load balance (Fig. 3(c)) has 6 axes, but in this work are used and calibrated only 3 axes relative to the lift, the drag and the pitching moment.

The pressure acquisition system (Fig. 5(a)) is a Scandaq 8000, that measure 64 pressure taps simultaneously with a piezoresistive sensor array; this acquisition system is used with a dedicated wing section. The sensors full scale is of

Fig. 2. The Subsonic Wind Tunnel at the Department of "Energetica" of the University "Politecnica delle Marche".

Fig. 3. The IR thermographic camera (a) , the IR window (b) and the 6 axis Load Balance (c).

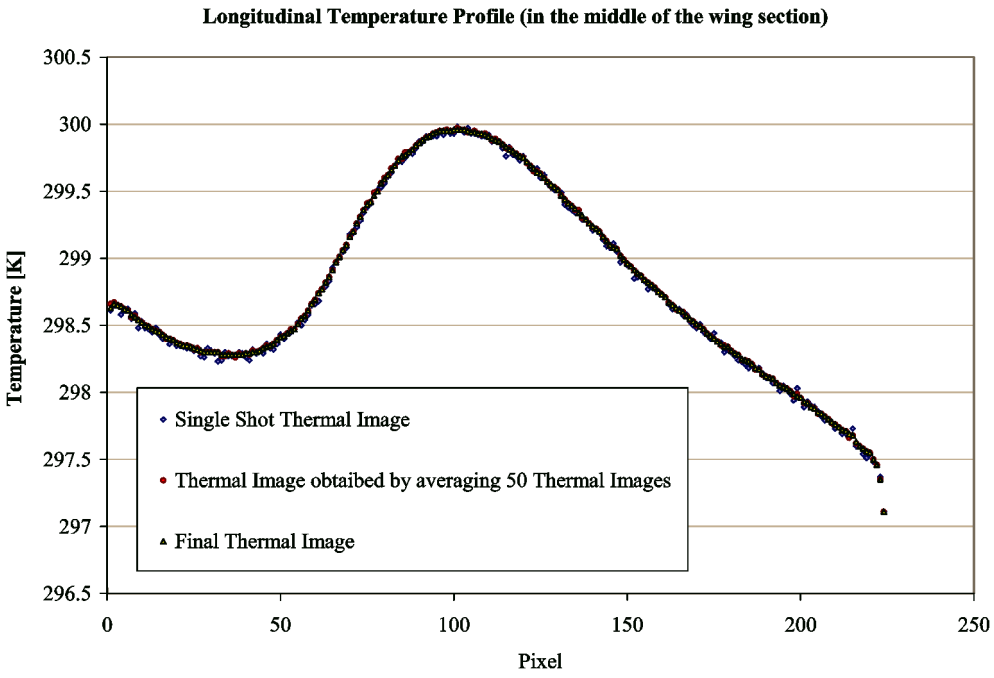

Fig. 4. Thermal Images Manipulations carried out by using the Matlab procedure.

2.5 kPa and the static accuracy is of ±0.2% FS in the worse case.

Two different wing sections are realized to carry out the experimental measures; both the sections are based on the same RR3823HL airfoil, that is used with good results in hand launching applications and works typically at low Reynolds numbers. The aerodynamic parameters are under reported:

- max. Thickness: 8.35%;
- max. Thickness chord position: 22.54%;
- max. Camber: 3.38%;
- max. Camber chord position: 39.12%.

This airfoil is subjected to the presence of the laminar separation bubble, but the forward max camber and max thickness positions allow an earlier transition at high angles of attack reducing the drag increase due to the bubble presence.

The wing sections are obtained by means of a cutting machine (Fig. 5(b)) that realizes the extrados and intrados moulds following two lateral CNC cutted dimes; this allows to build different wing sections with a good reproducibility and a good accuracy in the airfoil nose. The first wing section is used to analyze the C_p distribution and so is equipped with 60 pressure taps placed over the extrados and intrados in the middle section of the wing. The second section is ded-

Fig. 5. The Multipressure Scan System (a) and the Airfoil Section cutting machine (b).

icated to the load balance measures and to the thermographic analyses; in order to carry out the thermographic measures the wing is filled by a thermal insulate and the surface is coated with an adhesive aluminium foil 25 micron thick. The metallic coating is electrically supplied with an high current – low voltage generator; in this way it forms a uniform heat plane by Joule effect and the wing surface is more clearly revealed with respect to the background by the IR camera. This technique is named "heated-thin foil technique" and was previously tested and verified by other authors [15–20].

3. The numerical and analytical approach

The points characterizing the laminar buble are essentially three: the laminar separation point, the free shear layer transition and the turbulent reattachment point.

The laminar separation point, that will be called B_S, corresponds to the point with a zero first derivative in the velocity profile near the wall; to individuate this point it is necessary to resolve the equations describing the flow field inside the boundary layer. There are two different approaches for this problem: the similarity solutions and the monoparametric integral methods. In the former case it is assumed that the velocity profiles have the same shape inside the boundary layer in the streamwise direction; the Falkner–Skan formula (Eq. (1)) describes the inviscid flow over a wedge having an opening angle of $\beta\pi/2$ and is used as a good reference for boundary layers in the presence of pressure gradients [21,22].

$$U(x) = Kx^m, \qquad \eta = y\sqrt{\frac{m+1}{2}\frac{U_e(x)}{\nu x}}$$
$$\beta = \frac{2m}{m+1} \tag{1}$$

In the latter case the boundary layer equations are rewrited using an integral approach (Eq. (2)) and the velocity profile is directly imposed; in this way there is a unique parameter that describes the shape and the value of variables as the thickness displacement, the momentum thickness etc. In this research work the analyses are carried out by means of the Λ Polhausen parameter (Eq. (3)) with a polynomial velocity profile, that accounts the adverse pressure gradients typical of an airfoil surface and that allows to localize the separation point for a Λ value of -12 (Fig. 6).

$$\frac{\mathrm{d}}{\mathrm{d}x}(U_e^2\theta) + \delta^* U_e \frac{\mathrm{d}U_e}{\mathrm{d}x} = \frac{\tau_w}{\rho}$$
$$\delta^* = \int_0^\delta \left(1 - \frac{u}{U_e}\right)\mathrm{d}y$$
$$\theta = \int_0^\delta \frac{u}{U_e}\left(1 - \frac{u}{U_e}\right)\mathrm{d}y, \qquad H = \frac{\delta^*}{\theta} \tag{2}$$
$$\Lambda = \frac{\delta^2}{\nu}\frac{\mathrm{d}U_e}{\mathrm{d}x} \tag{3}$$

To obtain the Λ values along the RR3823HL curvilinear abscissa it is used the X foil software, that evaluates the shape parameter H (Eq. (2)); in fact this is related to the Λ value by means of the subsequent relation (Eq. (4)):

$$\Lambda = \frac{a + cH^2 + eH^4}{1 + bH^2 + dH^4}$$
$$a = 104.8826476$$
$$b = 0.407940445$$
$$c = -40.0527133$$
$$d = -0.13216036$$
$$e = 3.676751625 \tag{4}$$

The separation points B_S corresponding to the $\Lambda = -12$ value are so carried out for angles of attack between $-5°$ and $12°$ and for all the tested Reynolds numbers.

Once localized the laminar separation point it is also determined the transition point B_T inside the free shear layer, where the turbulent spots coalesce inducing a fully turbulent flow. The Xfoil software utilizes the e^9 criteria introduced by Michel (1952) and subsequently modified by Smith–Gamberoni (1956), Van Ingen (1956) and Jaffe (1970); the first author observed from the experimental available data that the transition point corresponds to a total amplification rate of the Tollmien–Schlichting waves in the order of $A/A_0 \approx 10^4$ [23,24]. On this base the other authors have

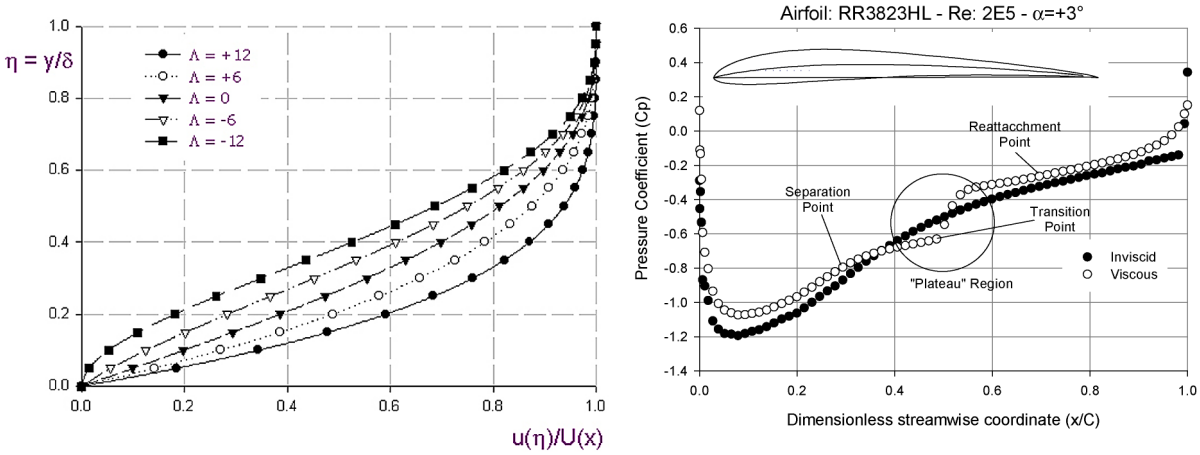

Fig. 6. Velocity Profiles depending on the Λ Polhausen parameter (a) The turbulent reattachment point individuation (b).

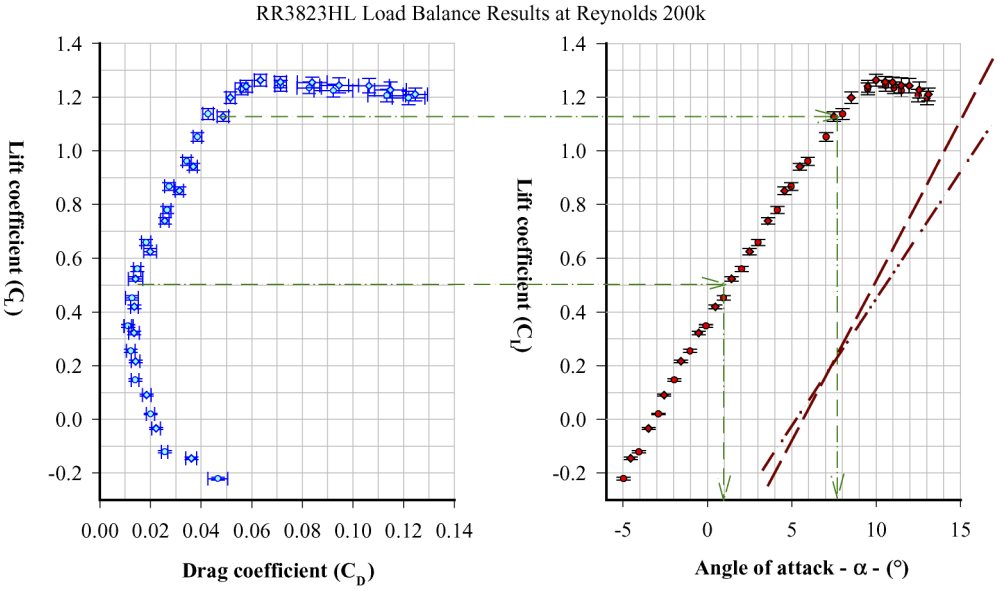

Fig. 7. RR3823HL Load Balance results at Reynolds 200k.

evaluated the eigenvalues of different boundary layers and have estimated the global growth of waves of given frequency. This has brought to the subsequent result:

$$\frac{A}{A_0} = \exp\left[\int_{x_i}^{x_r} \alpha c_i \, \mathrm{d}t\right] \approx e^9 \quad \begin{array}{l}\text{Smith–Gamberoni–}\\ \text{Van Ingen temporal}\\ \text{amplification}\end{array} \tag{5}$$

Together with values obtained by the X foil, the B_T points are also carried out by means of the Horton criteria [23]; this allows to quantify the distance L_T between the separation point and the transition point inside the free shear layer for a laminar bubble.

$$\frac{L_T}{\theta_{\text{sep}}} = \frac{C \times 10^4}{Re_{\theta,\text{sep}}} \quad 3 < C < 5 \tag{6}$$

The turbulent reattachment point is evaluated by X foil using the Swafford relation and, by a graphical method, observing the point over which the c_p viscous and the inviscid analysis shows the same trend (Fig. 6(b)).

4. Experimental results

The experimental tests are preliminary conducted by using the measurement systems used in the aerodynamic field; i.e. the load balance and the c_p distribution analysis. Subsequently the thermographic analyses are carried out for a more accurate laminar bubble study. All the tests were realized for angles of attack between $-5°$ and $12°$ and for four different Reynolds numbers: 60k, 100k, 150k, 200k.

Only for simplicity will be reported in this work the results related to the Reynolds 200k test.

In Fig. 7 are reported the Eiffel polar and the Lift vs. angle of attack curve obtained by using the load balance (the error bar reported in the graph are referred to the 2σ method). The laminar bubble presence may be deducted for an angle range between $1°$ and $8°$ by observing the C_L–C_D curve; this is because there is an anomalous drag increase underlined by a different trend concavity in this zone. The possible presence

of a laminar separation bubble is revealed also by observing the C_L vs. alfa curve; in fact there is a slope change (referring to the graph, the dashed line shows the slope before $-1°$ and the dash-dot-dot line shows the slope for angles higher than $-1°$) normally related to the presence of a large bubble in the airfoil center zone. This LB early growth toward the trailing edge and subsequently, by increasing the angle of attack, moves toward the leading edge and reduces its longitudinal extension.

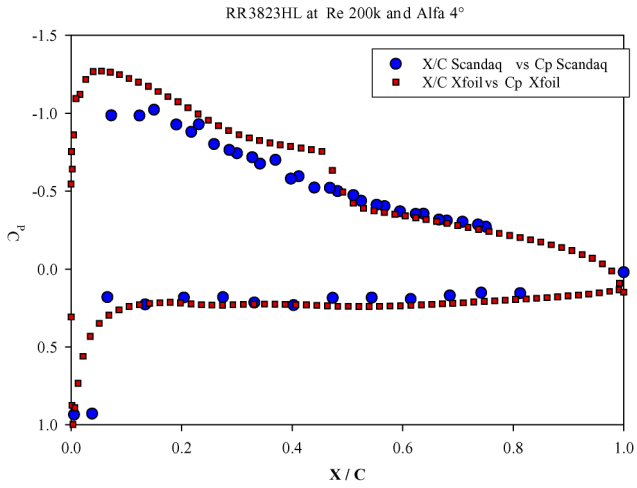

Fig. 8. Comparison on the Pressure Coefficient Distribution between numeric (XFOIL) and experimental (Scandaq) results.

Contrarily with the Eiffel polar observation the laminar bubble seems to be present starting from angles of $-1°$ but, as will be later explained, this results is confirmed by the IR thermography; it is so possible to deduct that for angles between $-1°$ and $1°$ the bubble has a noticeable longitudinal extension but it do not induce an appreciable pressure drag increase.

The c_p distribution trends obtained by using both the Scandaq measurement system and by means of the X foil analysis are reported in Fig. 8; the experimental data are in good agreement with the numerical results but underline a great difficulty to clearly distinguish the pressure behaviour inside the bubble.

The thermographic images obtained for the Reynolds 200k at different angles of attack are reported in Fig. 9; as previously described, every thermogram is carried out first by averaging 50 images acquired at a frequency of 8 Hz then subtracting the resulting thermogram with a reference

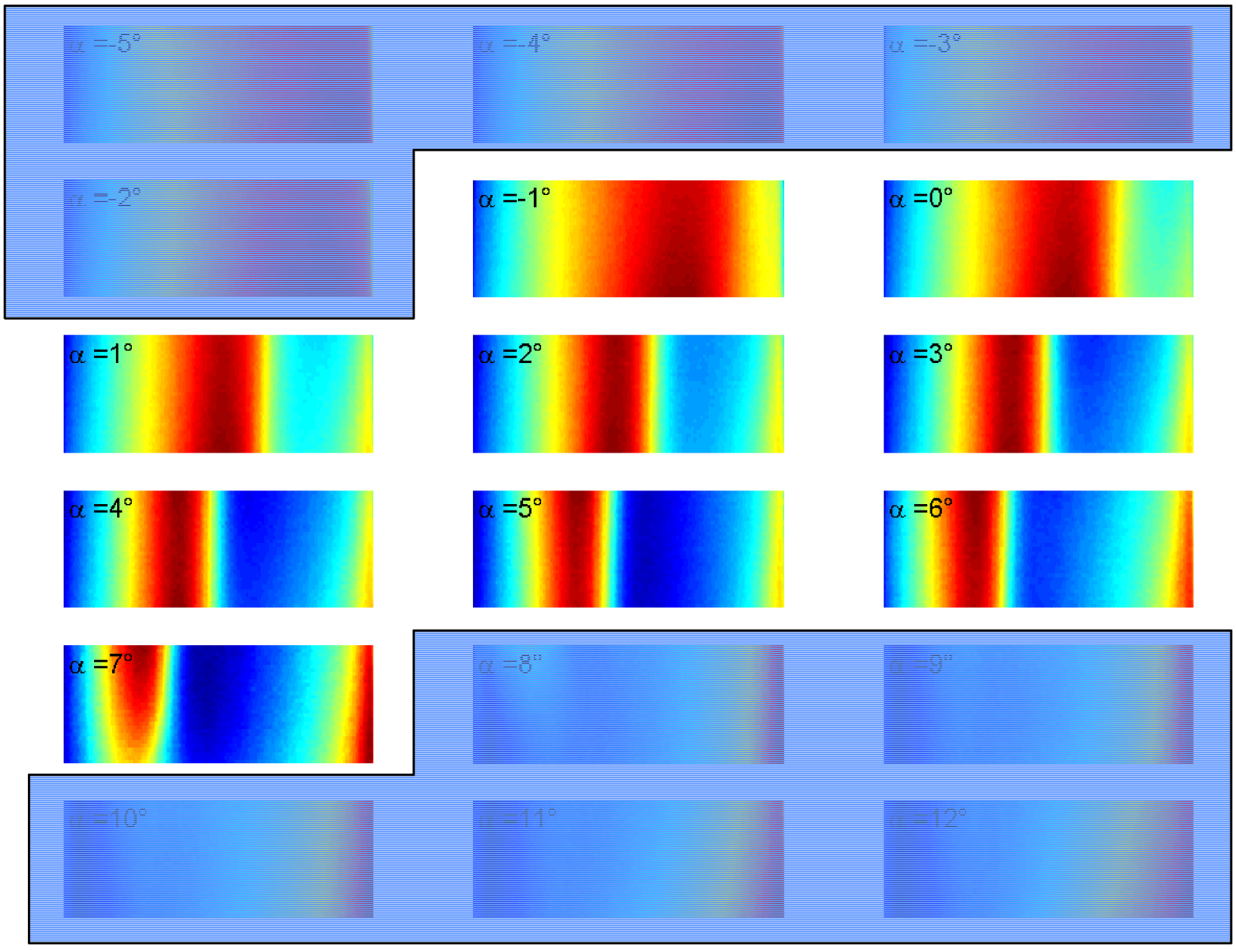

Fig. 9. RR3823HL Thermographic Images at Re 200k and for angles ranging from $-2°$ to $12°$.

image obtained by observing the heated wing section with the wind tunnel turned off. The bubble presence is qualitatively localized in the thermal IR image as a warmer zone; this happens because the surface heating is kept constant and uniform by regulating the current flux inside the metallic coating. In this way the surface temperature distribution is the unique function of the convective heat transfer coefficient and the presence of a laminar bubble, with a quasi static recirculating flow inside it, induces a local convective h coefficient decrease and so a temperature increase. This qualitative approach was verified in the previous work [14] and for the RR3823HL airfoil shows a range of angles of attack between $-1°$ and $7°$ where a laminar bubble is present. Particularly for angles between $-1°$ and $2°$ the bubble decreases its extension but the laminar separation point seems to be stationary; for angles between $3°$ and $7°$ there is a further longitudinal extension decrease and the L_S point moves toward the leading edge.

For a quantitative infrared analysis it is necessary to elaborate the temperature data obtained from the thermograms, in order to carry out the trend of the Stanton number; this because the St adimensional number is directly related to the surface convective heat transfer coefficient but allows also for the velocity distribution influence. As procedure, first the h values on the central longitudinal wing section are evaluated by an energy balance on a surface volume corresponding to a pixel; assuming a transversal symmetry the energy balance (Fig. 10) should consider the conductive heat transfer in the longitudinal direction, the internal heat generation by Joule effect, the radiative thermal dissipation and the convective heat exchange.

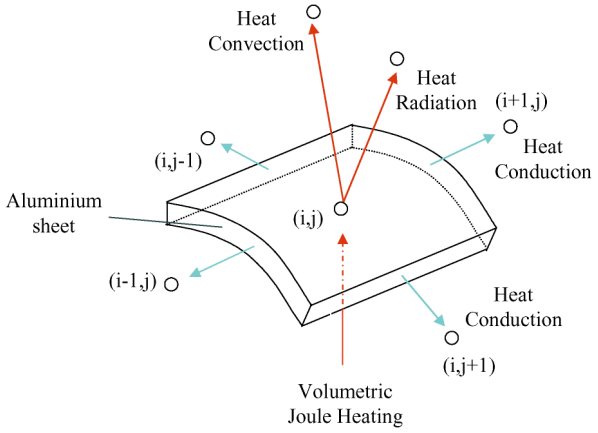

Fig. 10. The finite difference approach used to correct the temperature map.

$$\frac{T(i+1,j)-T(i,j)}{\frac{\Delta x}{\lambda s \Delta y}}+\frac{T(i-1,j)-T(i,j)}{\frac{\Delta x}{\lambda s \Delta y}}+\frac{T(i,j+1)-T(i,j)}{\frac{\Delta y}{\lambda s \Delta x}}+\frac{T(i,j-1)-T(i,j)}{\frac{\Delta y}{\lambda s \Delta x}}+h\Delta x\Delta y\big(T_\infty-T(i,j)\big)+\sigma\frac{T_{\text{surr}}^4-T^4(i,j)}{\frac{1-\varepsilon}{\varepsilon\Delta x\Delta y}+\frac{1}{F_{12}\Delta x\Delta y}+\frac{1-\varepsilon_{\text{surr}}}{\varepsilon_{\text{surr}}A_{\text{surr}}}}+G\Delta x\Delta y s=0 \quad (7)$$

The IR camera observes the wing section pixels with different view factors due to the airfoil curvature; in addition the wing section is rotated when the flow angle of attack is changed. To account the error deriving from the airfoil curvature a comparison with the equivalent flat plate inclined at the same angle is performed (Fig. 11); the result shows a maximum percent difference of 3% by excluding the airfoil nose zone up to the 2% of the chord.

In the h coefficient analysis is evaluated also the view factor influence on the IR camera detection with respect to the wing section surface; in Fig. 12 it is possible to observe that a view factor variation induces a convective heat transfer coefficient change with relation to its absolute value but does not modify the h trend and consequently the St trend. So it is possible to obtain again the positions of the B_S, B_T and B_R points that are deduced directly from the St trend.

To enhance with a greater detail the Stanton number variations along the longitudinal section it is decided to calculate the St values with the $U_e(s)$ velocity that the flow assumes outward the boundary layer along the curvilinear abscissa instead of the U_∞ velocity of the free stream flow. The $U_e(s)$ velocity is directly evaluated by using the X foil software

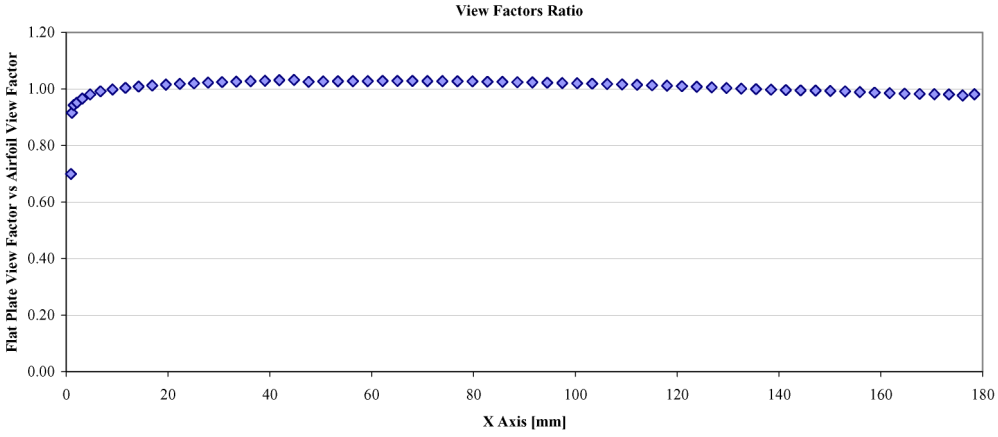

Fig. 11. View factor error evaluation.

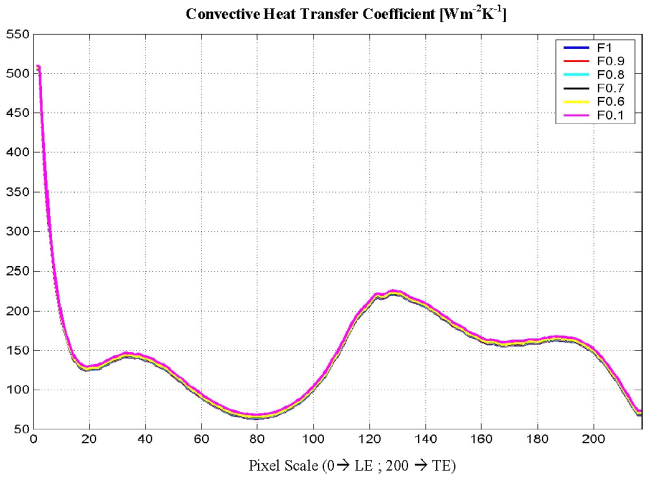

Fig. 12. Dependence on the view factor at $Re\,200k$ & 4°.

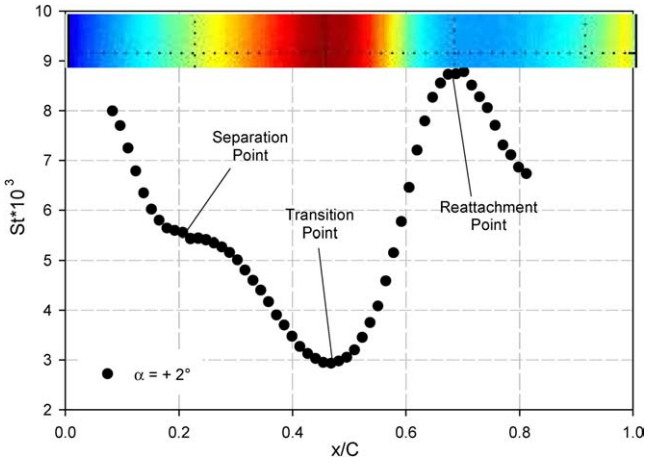

Fig. 13. Stanton number vs airfoil chord.

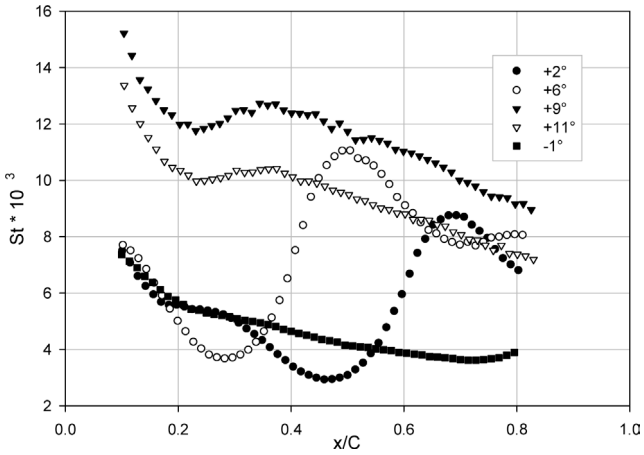

(a)

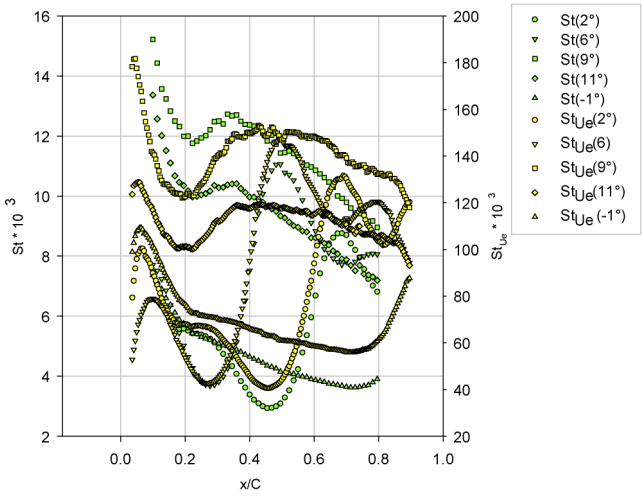

(b)

Fig. 14. (a) Stanton distribution at different angles of attack for *Re* 200*k*. (b) *St* and St_{U_e} distribution at different angles of attack for *Re* 200*k*.

for an inviscid flow on the tested airfoil; the choice to evaluate an inviscid flow derives from the consideration that the velocity calculated with this approach is univocally determined apart from the software used. Once obtained the St_{U_e} (Fig. 13) trend, the laminar separation point B_S is localized as the flex point that comes first the absolute minimum; i.e. the laminar separation represents a fluid dynamic singularity and this reflects too in a singularity for the thermal heat exchange. The B_T transition point is localized in the absolute minimum St_{U_e} value because it corresponds to the point of maximum bubble height where the convective heat transfer coefficient reaches a low value. The turbulent reattachment point is similarly individuated for the maximum heat transfer coefficient because the flow behaves like a jet impingement that maximizes the thermal dissipation.

On the basis of this approach the St_{U_e} trend is carried out in the central wing section at different angles of attack; as it is possible to observe in Fig. 14, a behaviour similar to the one previously described is easily recognizable for α between 2° and 6°, whereas is more difficult to individuate at $\alpha - 1°$ and it is not observable for angles of 9° and 11°.

It is possible to better understand the laminar bubble behaviour both collecting in more graphs (Fig. 15) the characteristic bubble points positions by varying the angle of attack and the Reynolds number and evaluating indirectly the bubble longitudinal dimension as difference between the B_S and the B_R. The laminar separation point tendentially moves toward the airfoil leading edge but it is stationary for angles around 2°; this behaviour may be due to the movement of the aspiration peak, and so of the adverse pressure gradient, toward the leading edge by increasing the alfa value and is confirmed by the numerical prediction of the integral approach to the boundary layer solution. Also the transition point and the turbulent reattachment point move toward the leading edge by increasing alfa; similarly to the previous case there is a good correspondence between the experimental results and the numerical predictions, with a particular reference to the Horton relation. Globally the laminar bubble reduces its longitudinal extension by increasing alfa and shows a substantial independence to the Reynolds number; this is not strictly true for the lower tested Reynolds (60*k*) where the bubble is present everywhere with an higher extension.

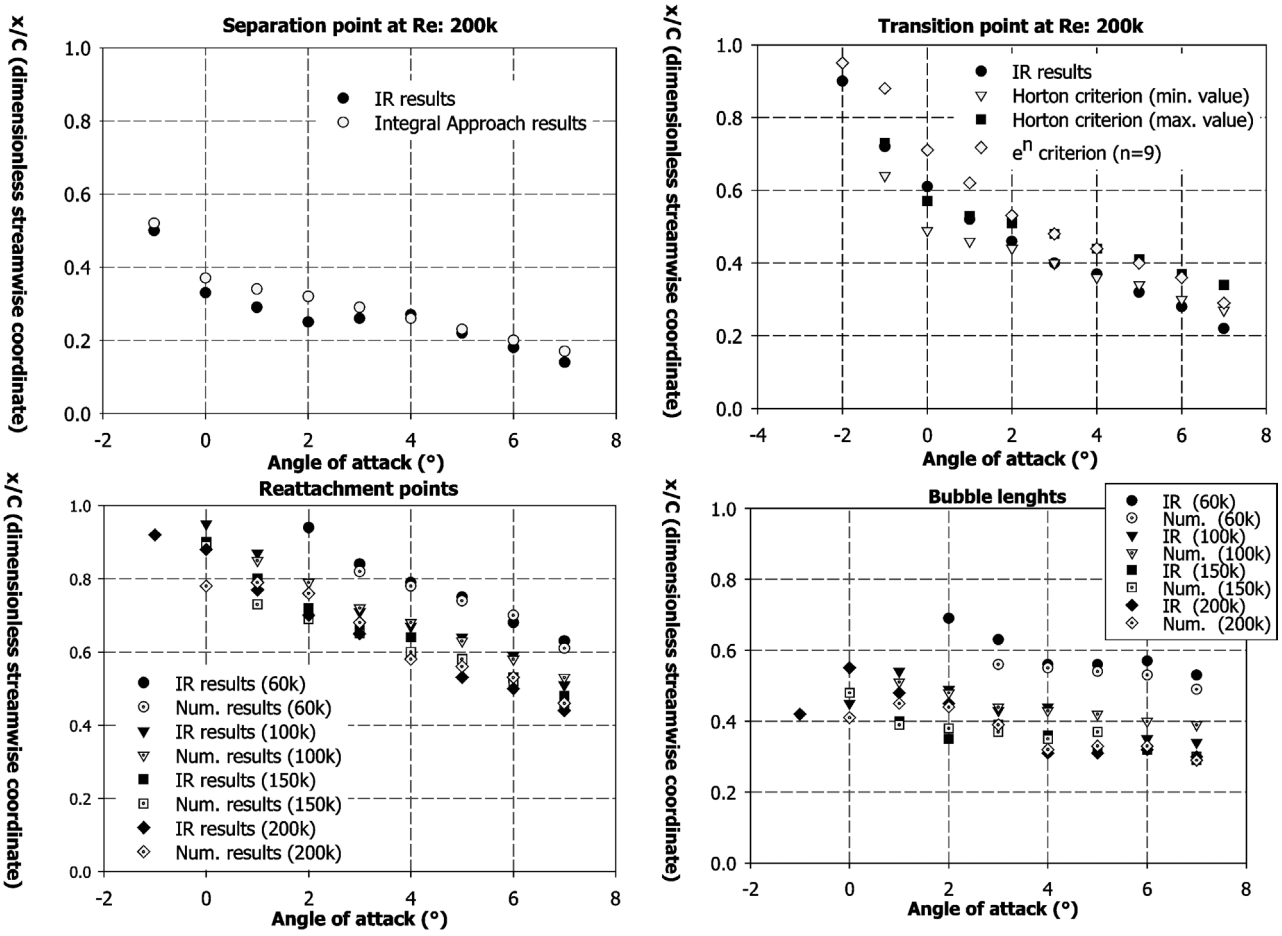

Fig. 15. Laminar bubble behaviour varying the airfoil angle of attack.

Table 1
Summary table

Alfa	Laminar separation			Transition				Reattachment		Bubble lenght		Reδ2(Sep.)	Reδ2(Tr.)	Reδ2(Tr.)	Reδ2(Tr.)
	($L=-12$)	($L=-10$)	IR	Tr.(min)	Tr.(max)	Tr.(X foil)	Tr.(IR)	X foil	IR	Num	IR		X foil	min	max
−2	Unsep.	Unsep.	Unsep.			0.95	0.90	Unsep.	Unsep.	Unsep.	Unsep.				
−1	0.52	0.44	0.50	0.64	0.73	0.88	0.74	?	0.92	?	0.42	258	354	293	314
10	0.37	0.34	0.39	0.49	0.57	0.71	0.61	0.78	0.88	0.41	0.49	225	343	266	290
1	0.34	0.32	0.29	0.46	0.53	0.62	0.52	0.79	0.77	0.45	0.48	216	300	260	280
2	0.32	0.30	0.26	0.44	0.51	0.53	0.47	0.76	0.70	0.44	0.44	220	288	260	285
3	0.29	0.26	0.29	0.40	0.48	0.48	0.42	0.68	0.65	0.39	0.36	217	281	255	280
4	0.26	0.24	0.26	0.36	0.44	0.44	0.36	0.58	0.58	0.32	0.32	213	274	255	280
5	0.23	0.21	0.22	0.34	0.41	0.40	0.32	0.56	0.53	0.33	0.31	210	274	252	280
6	0.20	0.18	0.18	0.30	0.37	0.36	0.29	0.53	0.50	0.33	0.32	206	270	250	285
7	0.17	0.14	0.13	0.27	0.34	0.29	0.22	0.46	0.44	0.29	0.31	202	260	250	380

5. Conclusions

This research aimed to extend the IR thermographic technique for a quantitative study of the laminar bubble phenomenon. Once in a previous work [14] was verified the possibility to use the IR thermography for a qualitative investigation of the laminar bubble behaviour. This phenomenon occurs mainly at low Reynolds number and induces an airfoil drag increase and sometime a lift decrease; it derives the necessity to localize a bubble presence and to understand its behaviour. The standard aerodynamic techniques are able to underline the possible presence of a local boundary layer separation but are not able to fully characterize the bubble behaviour and sometimes are not so refined to localize phenomena having low influence on the lift and drag parameters. The IR thermography seems instead able to supply more detailed information about the characteristic points of a laminar bubble: i.e. the laminar separation point B_S, the transition point in the free shear layer B_T, and the turbulent reattachment point B_R. In order to obtain quantitative information from

the thermographic data it is necessary to carry out a further analysis starting from the surface temperature distribution; first an energy balance on the different heat transfer contributions is to allow for. A distribution of the adimensional Stanton number is successively to carry out and an analysis of its trend should be performed to localize some mathematical characteristic points related to the laminar bubble describing points. Finally summarizing all the data about the B_S, B_T, B_R, and L_B in graphs depending on the angle of attack and the Reynolds number it is possible to better understand the bubble behaviour. For the tested RR3823HL airfoil the bubble phenomenon shows a movement toward the leading edge increasing the alfa values and it reduces its longitudinal extension all trough this movement. The laminar bubble behaviour seems to be lesser dependent on the Reynolds number apart from the lower tested *Re* of 60*k*.

Appendix A

$$C_L = \frac{L}{q_\infty S} \quad \text{wing lift coefficient}$$

$$C_D = \frac{D}{q_\infty S} \quad \text{wing drag coefficient}$$

$$C_{M,c/4} = \frac{M}{q_\infty Sc} \quad \text{wing pitching moment coefficient}$$

$$c_p = \frac{p - p_\infty}{q_\infty} \quad \text{pressure coefficient}$$

References

[1] Proceedings of the Conference on Low Reynolds Number Airfoil Aerodynamics, UNDAS-CP-77B123, Notre Dame, Indiana, June 1985.

[2] Proceedings of the Aerodynamics at Low Reynolds Numbers $10^4 < Re < 10^6$ International Conference, London, October 1986.

[3] Proceedings of the Conference on Low Reynolds Number Aerodynamics. The University of Notre Dame, Notre Dame, Indiana, June 1989.

[4] D. Althaus, Recent wind tunnel experiments at low Reynolds numbers, in: Proceedings of the Aerodynamics at Low Reynolds Number $10^4 < Re < 10^6$ International Conference, London, October 1986.

[5] D. Althaus, Profilpolaren für den Modellflug, Necker-Verlag, Villingen-Schwenningen, 1980.

[6] D. Althaus, Profilpolaren für den Modellflug, vol. 2, Necker-Verlag, Villingen-Schwenningen, 1985.

[7] I.H. Abbott, A.E. von Doenhoff, Theory of Wing Sections, Dover, New York, 1959.

[8] B.W. McCormick, Aerodynamics, Aeronautics and Flight Mechanics, Wiley, New York, 1979.

[9] R. Eppler, D.M. Somers, A computer program for the design and analysis of low-speed airfoils, including transition, NASA TM 80210, August 1980.

[10] R. Eppler, Airfoil Design and Data, Springer, New York, 1990.

[11] M.S. Selig, J.F. Donovan, D.B. Fraser, Airfoils at Low Speeds, Soartech 8, H.A. Stokely, Virginia Beach, 1989.

[12] C.A. Lyon, A.P. Broeren, P. Giguère, A. Gopalarathnam, M.S. Selig, Summary of Low-Speed Airfoil Data, vol. 3, Soartech Publications, 1997.

[13] M. Selig, Addendum to the design of airfoils at low Reynolds numbers, Soartech IV, January, 1985, pp. 30–65.

[14] S. Montelpare, R. Ricci, A thermographic method to evaluate the local boundary layer separation phenomena on aerodynamic bodies operating at low Reynolds number, Internat. J. Thermal Sci. 43 (2004) 315–329.

[15] G.M. Carlomagno, L. De Luca, G. Buresti, G. Lombardi, Characterization of boundary layer conditions in wind tunnel tests through IR infrared thermography imaging, in: T.L. Williams (Ed.), Applications of Infrared Technology, in: Proc. SPIE, vol. 599, 1988, pp. 23–29.

[16] G.M. Carlomagno, L. De Luca, Infrared thermography in heat transfer, in: W.I. Young (Ed.), Handbook of Flow Visualization, Hemisphere, 1989, pp. 531–533, Chapter 32.

[17] S. Montelpare, M. Paroncini, R. Ricci. P. Zazzini, Flow visualization of the laminar separation bubble by infrared thermography investigations, in: 5th International Workshop on Advanced Infrared Technology and Applications, Venezia, 29–30 September 1999.

[18] G. Latini, S. Montelpare, R. Ricci, Individuazione di fenomeni di separazione dello strato limite su corpi aerodinamici operanti a bassi numeri di Reynolds mediante l'uso della Termografia, in: 6° Convegno Nazionale di Ingegneria del Vento In-Vento 2000, Genova, 18–21 giugno 2000.

[19] S. Montelpare, R. Ricci, P. Zazzini, Laminar separation bubble visualisation by I.R. thermography, in: 9th International Symposium on Flow Visualization, Edinburgh, Scotland, 22–25 August 2000.

[20] G. Cesini, S. Montelpare, R. Ricci, P. Zazzini, Un metodo termografico per lo studio del fenomeno di separazione dello strato limite laminare in corpi operanti a basso numero di Reynolds, in: 56° Congresso Nazionale ATI, Napoli, 10–14 Septembre 2001.

[21] H. Schlichting, K. Gersten, Boundary Layer Theory, eighth revised ed., ISBN 3-540-66270-7, 2000.

[22] F.M. White, Viscous Fluid Flows, int. ed., ISBN 0-07-100995-7, 1991.

[23] H.P. Horton, A semi-empirical theory of the growth and bursting of laminar separation bubbles, Aero. Res. Counc. 107 (1967).

[24] J.L. Van Ingen, On the calculation of laminar separation bubbles in two-dimensional incompressible flow, AGARD Conf. Proc. Flow Separation 168 (1975).